Inorganic Chemistry

pubs.acs.org/IC Article

# Covalent Bonding of Salen Metal Complexes with Pyrene Chromophores to Porous Polymers for Photocatalytic Hydrogen Evolution

Shu-Ying Huang,[†] Xiao Lin,[†] Hao-Yu Yang, Xue-Rong Dou, Wen-Jie Shi, Ji-Hua Deng,* Di-Chang Zhong, Yun-Nan Gong,* and Tong-Bu Lu

Cite This: *Inorg. Chem.* 2024, 63, 13594−13601 Read Online

ACCESS | Metrics & More | Article Recommendations | Supporting Information

**ABSTRACT:** The development of low-cost and efficient photocatalysts to achieve water splitting to hydrogen ($H_2$) is highly desirable but remains challenging. Herein, we design and synthesize two porous polymers (Co−Salen−P and Fe−Salen−P) by covalent bonding of salen metal complexes and pyrene chromophores for photocatalytic $H_2$ evolution. The catalytic results demonstrate that the two polymers exhibit excellent catalytic performance for $H_2$ generation in the absence of additional noble-metal photosensitizers and cocatalysts. Particularly, the $H_2$ generation rate of Co−Salen−P reaches as high as 542.5 $\mu$mol $g^{-1}$ $h^{-1}$, which is not only 6 times higher than that of Fe−Salen−P but also higher than a large amount of reported Pt-assisted photocatalytic systems. Systematic studies show that Co−Salen−P displays faster charge separation and transfer efficiencies, thereby accounting for the significantly improved photocatalytic activity. This study provides a facile and efficient way to fabricate high-performance photocatalysts for $H_2$ production.

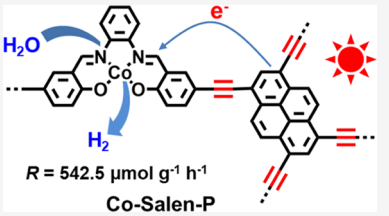


## INTRODUCTION

The large-scale usage of fossil fuels has resulted in a serious energy crisis and environmental pollution.[1,2] The development of green energy as a substitute for fossil fuels is of great significance.[3−10] Hydrogen ($H_2$), as a green, pollution-free, and high-energy-capacity fuel, is regarded to be an ideal substitute.[11−13] Recently, various technologies have been developed to produce $H_2$, among which photocatalytic $H_2$ evolution from water splitting driven by solar energy has garnered more and more attention because it can achieve everlasting solar-to-fuel conversion.[14−18] Therefore, the exploration of efficient photocatalysts to achieve this important reaction is considered one of the most critical issues.

Since Fujishima and Honda reported $TiO_2$ electrodes for photocatalytic $H_2$ production by water splitting in 1972, a large variety of semiconductors (e.g., metal oxides, metal chalcogenides, and perovskites) and semiconductor-like materials (e.g., metal−organic frameworks, covalent−organic frameworks, and hydrogen-bonded organic frameworks) have been prepared and applied in photocatalytic $H_2$ evolution.[19−28] However, these photocatalysts often exhibit low catalytic efficiency due to the fast recombination of photogenerated electron−hole pairs. To promote charge separation, the introduction of noble-metal Pt cocatalysts into a catalytic system has been proven a facile and effective strategy.[29−38] Nevertheless, the high cost and extreme scarcity of Pt seriously impede the large-scale practical applications. In this regard, it is highly desired to develop low-cost and high-performance photocatalysts for $H_2$ evolution.

Transition metal complexes have been widely used in photocatalytic $H_2$ evolution due to their well-defined and tailorable structures, maximized utilization of metal sites, and low cost.[39−44] Unfortunately, owing to the poor visible light harvesting ability of transition metal complexes, additional photosensitizers were always added to catalytic systems to improve catalytic efficiency. Moreover, pyrene-based compounds containing a $\pi$-conjugated system display splendid visible light harvesting ability, which are also used in photocatalysis.[45−48] Therefore, the integration of transition metal complexes and pyrene-based compounds in one system may be an outstanding strategy to obtain high-efficiency and low-cost catalysts for photocatalytic $H_2$ production. Herein, we rationally constructed two porous polymers (Co−Salen−P and Fe−Salen−P) by covalent bonding of salen metal complexes and pyrene chromophores for photocatalytic $H_2$ evolution. Interestingly, Co−Salen−P displays high photocatalytic performance for $H_2$ evolution with a $H_2$ production rate of 542.5 $\mu$mol $g^{-1}$ $h^{-1}$ in the absence of additional noble-metal photosensitizers and cocatalysts, 6-fold higher than that of Fe−Salen−P. Such high photocatalytic performance of Co−Salen−P can be attributed to its fast charge separation and transfer, as

Received: April 29, 2024
Revised: June 27, 2024
Accepted: June 28, 2024
Published: July 8, 2024

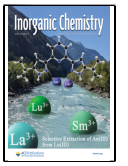







https://doi.org/10.1021/acs.inorgchem.4c01774
*Inorg. Chem.* 2024, 63, 13594−13601

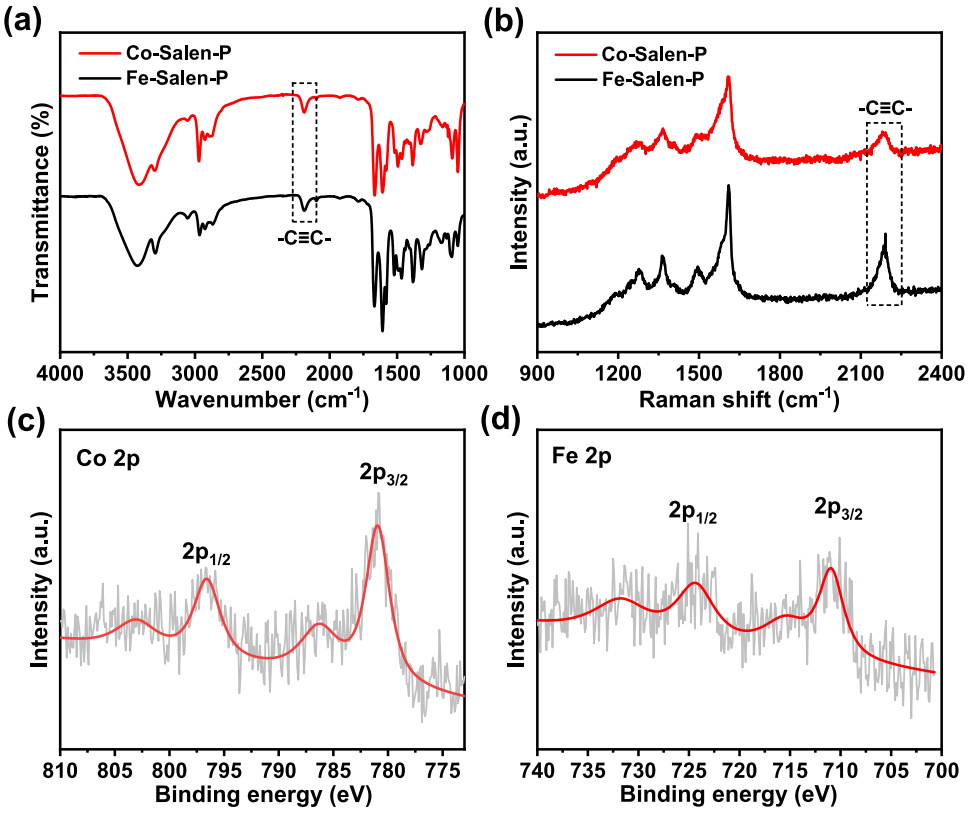


**Figure 1.** (a) FTIR spectra of Co−Salen−P and Fe−Salen−P. (b) Raman spectra of Co−Salen−P and Fe−Salen−P. (c) XPS spectrum for the Co 2p of Co−Salen−P. (d) XPS spectra for the Fe 2p of Fe−Salen−P.

demonstrated by a series of photo/electrochemical experiments. To the best of our knowledge, the photocatalytic activity of Co−Salen−P is superior to a large amount of reported Pt-assisted photocatalytic systems.

## RESULTS AND DISCUSSION

The salen ligand ($H_2L$) was first synthesized by a Schiff base reaction of o-phenylenediamine and 5-bromo-2-hydroxybenzaldehyde at room temperature.[49] The result of the $^1H$ nuclear magnetic resonance (NMR) spectrum shows that $H_2L$ was successfully obtained with high purity (Figure S1). Then, the M−Salen complexes (M = Co and Fe) were prepared by reaction of $H_2L$ and $Co(ClO_4)_2{\cdot}6H_2O$/$Fe(ClO_4)_3{\cdot}H_2O$.[49] Liquid chromatography-mass spectrometry (LC-MS) of Co−Salen shows a strong ion peak at $m/z$ 605.87, corresponding to the species of $\{[CoL(CH_3CN)(CH_3OH)] + H^+\}$ (Figure S2). For the Fe−Salen complex, two strong ion peaks at 527.86 and 568.88 were observed, which can be assigned to $[FeL]^+$ and $[FeL(CH_3CN)]^+$, respectively (Figure S3). Subsequently, Co−Salen−P and Fe−Salen−P polymers were synthesized via a Sonogashira−Hagihara C−C coupling reaction between M−Salen complexes and 1,3,6,8-tetraethynylpyrene (Scheme S1). Fourier transform infrared spectroscopy (FTIR) of Co−Salen−P and Fe−Salen−P show characteristic peaks at 2190 and 2189 $cm^{-1}$, respectively, corresponding to unsymmetrical alkyne bonds (−C≡C−; Figure 1a).[50,51] Raman spectra of Co−Salen−P and Fe−Salen−P exhibit characteristic peaks at 2187 and 2191 $cm^{-1}$, respectively, which are also assigned to the unsymmetrical alkyne bonds (−C≡C−; Figure 1b).[50,51] These results show the presence of alkynyl linkages in the two materials, suggesting the successful preparation of Co−Salen−P and Fe−Salen−P polymers. Powder X-ray diffraction (XRD) patterns of Co−Salen−P and Fe−Salen−P show amorphous natures (Figure S4).

The chemical compositions of Co−Salen−P and Fe−Salen−P were investigated by energy dispersive spectroscopy (EDS) mapping and X-ray photoelectron spectroscopy (XPS). The EDS mapping reveals the homogeneous distribution of C, N, O, and Co in Co−Salen−P and C, N, O, and Fe in Fe−Salen−P (Figures S5 and S6). The XPS spectra show C, N, O, and Co binding energies in Co−Salen−P and C, N, O, and Fe binding energies in Fe−Salen−P, which are consistent with the EDS results (Figures S7 and S8). Moreover, no obvious Br binding energy was observed in the XPS spectra of Co−Salen−P and Fe−Salen−P (Figures S7 and S8). These results further confirm the formation of Co−Salen−P and Fe−Salen−P polymers. The Co and Fe oxidation states were determined by XPS. As shown in Figure 1c, the Co 2p XPS spectrum of Co−Salen−P exhibits two characteristic peaks at 781.0 and 796.6 eV, which can be assigned to the binding energies of Co $2p_{3/2}$ and Co $2p_{1/2}$, respectively. Moreover, two satellite peaks are also observed with binding energies of 786.2 and 803.1 eV, respectively, demonstrating that the Co oxidation state is +2.[52] For Fe−Salen−P, the Fe 2p XPS spectrum displays Fe $2p_{3/2}$ and Fe $2p_{1/2}$ characteristic peaks with binding energies of 711.0 and 724.4 eV, respectively. There are also two corresponding satellite peaks with binding energies of 715.5 and 731.7 eV, respectively, revealing that the Fe oxidation state is +3 (Figure 1d).[53] Additionally, the contents of Co, Fe, and Pd in the two polymers were determined by an inductively coupled plasma mass spectrometer (ICP-MS). For Co−Salen−P, the contents of Co and Pd were 4.3 and 1.1 wt %, respectively. For Fe−Salen−P, the contents of Fe and Pd were 5.5 and 0.79 wt %, respectively.


https://doi.org/10.1021/acs.inorgchem.4c01774
Inorg. Chem. 2024, 63, 13594−13601

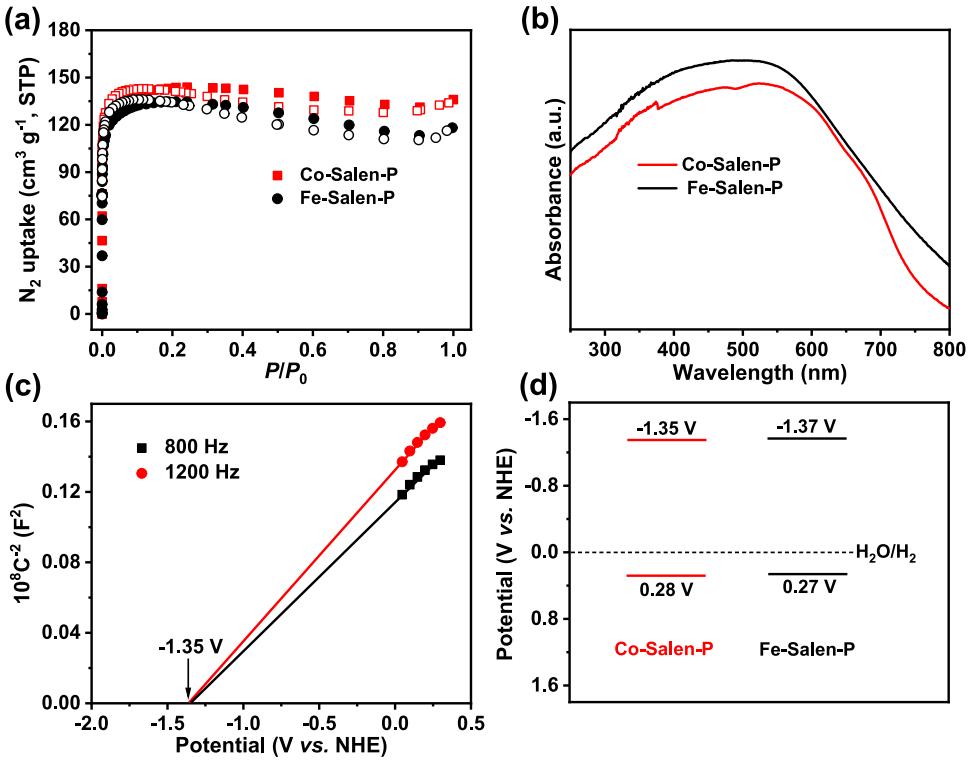


**Figure 2.** (a) $N_2$ adsorption isotherms of Co−Salen−P and Fe−Salen−P. (b) UV−vis spectra of Co−Salen−P and Fe−Salen−P. (c) Mott−Schottky plots of Co−Salen−P. (d) Band-structure diagram for Co−Salen−P and Fe−Salen−P.

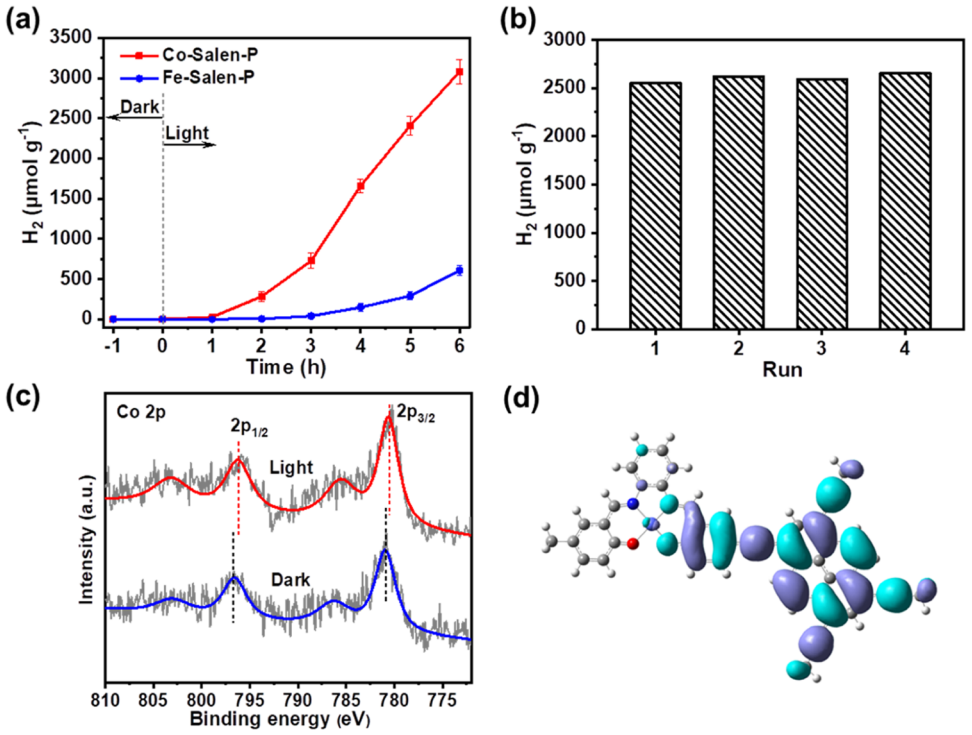


**Figure 3.** (a) Time-dependent photocatalytic $H_2$ evolution over Co−Salen−P and Fe−Salen−P. (b) The photocatalytic $H_2$ production rate of Co−Salen−P in four consecutive runs (5 h for each run). (c) XPS spectra for the Co 2p of Co−Salen−P in the dark and upon light irradiation. (d) The HOMO of Co−Salen−P.

The porous feature of Co−Salen−P and Fe−Salen−P was evaluated by a $N_2$ adsorption experiment. As shown in Figure 2a, the $N_2$ adsorption isotherms of Co−Salen−P and Fe−Salen−P at 77 K and 1 atm unveil typical type-I curves, suggesting their microporous characteristic. Their saturated $N_2$ uptake values are 136.3 and 118.2 $cm^3\ g^{-1}$ (STP), respectively, corresponding to the Brunauer−Emmett−Teller (BET) surface areas of 562.4 and 531.9 $m^2\ g^{-1}$, respectively.



https://doi.org/10.1021/acs.inorgchem.4c01774
Inorg. Chem. 2024, 63, 13594−13601

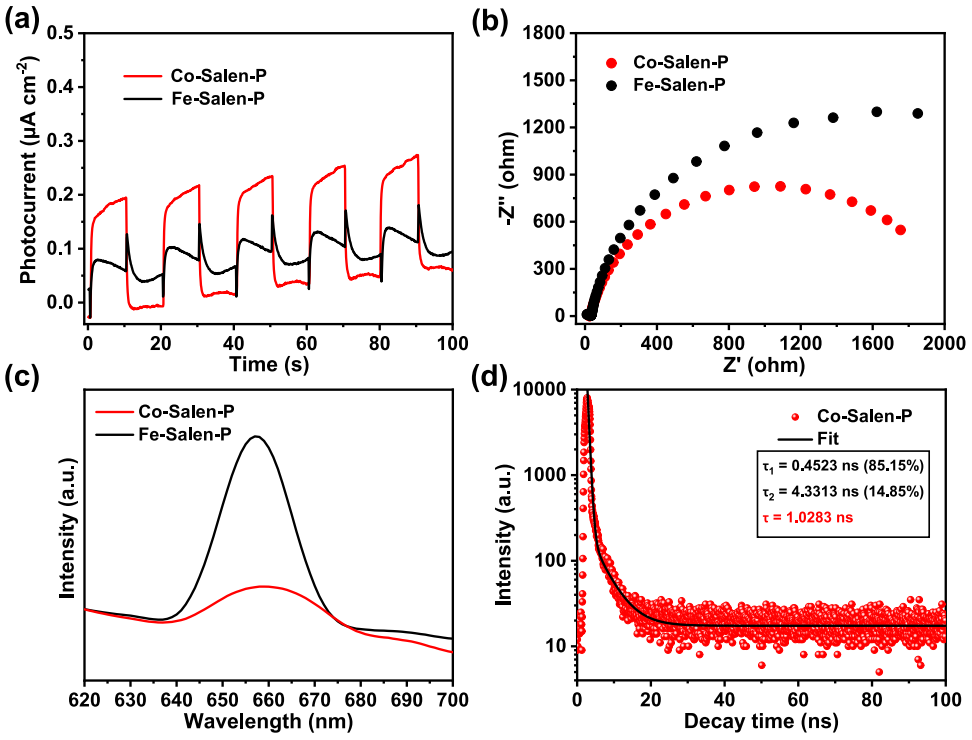


**Figure 4.** (a) Photocurrent response of Co−Salen−P and Fe−Salen−P. (b) EIS spectra of Co−Salen−P and Fe−Salen−P. (c) PL spectra of Co−Salen−P and Fe−Salen−P under excitation at 440 nm. (d) Transient fluorescence lifetime of Co−Salen−P.

Furthermore, they display the same pore size of 0.49 nm, revealing that they are indeed microporous materials (Figures S9 and S10). Additionally, the results of thermogravimetric analysis (TGA) demonstrate that both Co−Salen−P and Fe−Salen−P show weight loss from 130 to 200 °C, which may be attributed to the removal of the *N*,*N*-dimethylformamide (DMF) molecule. The desolvated Co−Salen−P and Fe−Salen−P exhibit hardly any weight loss up to 500 °C, demonstrating their high thermal stability (Figure S11).

To investigate the light harvesting ability, the solid ultraviolet−visible (UV−vis) spectra of Co−Salen−P and Fe−Salen−P were carried out. As shown in Figure 2b, they can absorb both ultraviolet and visible light with intrinsic absorption edges up to 800 nm. Their band gap energies ($E_g$) are 1.63 and 1.64 eV, respectively, which are calculated by the Kubelka−Munk (KM) method based on solid UV−vis spectra (Figures S12 and S13).[54] Their lowest unoccupied molecular orbitals (LUMOs) are determined by the results of Mott−Schottky measurements at frequencies of 800 and 1200 Hz, which are −1.35 and −1.37 versus NHE, respectively (Figures 2c and S14). It is worth noting that Co−Salen−P and Fe−Salen−P show the positive slopes of the $C^{2-}$ values (vs applied potentials), demonstrating that they are n-type semiconductors. Therefore, their highest occupied molecular orbitals (HOMOs) are calculated to be 0.28 and 0.27 V versus NHE, respectively. Obviously, the LUMOs of Co−Salen−P and Fe−Salen−P are more negative than that of proton reduction (0 V vs NHE), suggesting that they are theoretically feasible for photocatalytic $H_2$ evolution (Figure 2d).[55]

On the basis of the above results, the photocatalytic $H_2$ evolution over Co−Salen−P and Fe−Salen−P was investigated in $CH_3CN/H_2O$ (v/v = 4:1) with ascorbic acid as the sacrificial agent and in the absence of additional noble-metal photosensitizers and cocatalysts. After 6 h of light irradiation, the $H_2$ yields of Co−Salen−P and Fe−Salen−P are 3254.9 and 547.7 $\mu$mol $g^{-1}$ (related to production rates of 542.5 and 91.3 $\mu$mol $g^{-1}$ $h^{-1}$), respectively (Figure 3a). Obviously, Co−Salen−P displays an about 6 times higher $H_2$ evolution rate than that of Fe−Salen−P. Moreover, the $H_2$ evolution rate of Co−Salen−P is higher than a lot of reported Pt-assisted photocatalytic systems (Table S1). Furthermore, the photocatalytic $H_2$ evolution of Co−Salen/1,3,6,8-tetrabromopyrene constructed by a physical mixture of Co−Salen and 1,3,6,8-tetrabromopyrene was performed under the same catalytic condition. The result showed that a negligible amount of $H_2$ was detected, suggesting that covalent bonding of the metal complex and pyrene chromophores is an outstanding strategy to boost photocatalytic performance. In addition, the photocatalytic $H_2$ evolution of Salen−P constructed by the reaction of $H_2L$ and 1,3,6,8-tetraethynylpyrene was carried out. The result demonstrates that the $H_2$ production rate was only 0.047 $\mu$mol $g^{-1}$ $h^{-1}$, suggesting the Co in Co−Salen−P and Fe in Fe−Salen−P were the catalytic sites to achieve photocatalytic $H_2$ evolution (Figure S15). The photocatalytic durability of Co−Salen−P was evaluated by recycling experiments. During the four consecutive runs, the $H_2$ evolution rates of Co−Salen−P hardly changed, revealing its high catalytic stability (Figure 3b). The results of FTIR spectra show that Co−Salen−P and Fe−Salen−P still present the characteristic peaks of the unsymmetrical alkyne bonds (−C≡C−) at 2189 and 2190 $cm^{-1}$ after the photocatalytic reaction, unveiling their excellent structural stability (Figures S16 and S17). These results demonstrate that Co−Salen−P and Fe−Salen−P indeed possess high stability in the process of photocatalytic $H_2$ production. Additionally, a series of control experiments over Co−Salen−P show that no $H_2$ is detected in the absence of light, catalyst, and ascorbic acid, demonstrating that these factors are indispensable for photocatalytic $H_2$ evolution.



https://doi.org/10.1021/acs.inorgchem.4c01774
Inorg. Chem. 2024, 63, 13594−13601

The possible mechanism for photocatalytic $H_2$ evolution was elucidated by in situ XPS measurement and theoretical calculation. Taking Co−Salen−P as a representative, the Co 2p XPS spectrum displays two characteristic peaks at 781.0 (Co $2p_{3/2}$) and 796.6 eV (Co $2p_{1/2}$) in the dark, which shift to 780.5 and 796.1 eV, respectively, upon light illumination, suggesting that $Co^{2+}$ accepts the photogenerated electrons (Figure 3c). Moreover, density functional theory (DFT) calculations of Co−Salen−P were conducted to ascertain HOMO and LUMO positions.[56] As shown in Figures 3d and S18, the HOMO is located mainly in the pyrene group, and the LUMO lies on the Co−Salen complex. These results suggest that the Co−Salen−P harvests light to generate electrons and holes, where electrons shift from the pyrene group to the Co−Salen complex to reduce $Co^{2+}$ to $Co^{+}$. The $Co^{+}$ can further reduce $H^{+}$ to $H_2$. Additionally, the photogenerated holes are annihilated by an ascorbic acid sacrificial agent.

To elucidate the higher photocatalytic activity of Co−Salen−P than Fe−Salen−P, a series of photo/electrochemical measurements containing photocurrent response, electrochemical impedance spectroscopy (EIS), photoluminescence (PL) emission, and time-resolved PL (TRPL) spectra were conducted.[57,58] As shown in Figure 4a, Co−Salen−P exhibits a higher photocurrent response than Fe−Salen−P, implying the faster separation of photogenerated electron−hole pairs. The results of EIS demonstrate that Co−Salen−P possesses a smaller semicircle radius, revealing the lower charge-transfer resistance (Figure 4b). The PL spectra demonstrate that the emission intensity of Co−Salen−P is weaker than that of Fe−Salen−P, suggesting faster electron transfer (Figure 4c). Moreover, the results of TRPL show that Co−Salen−P displays a larger PL average lifetime than Fe−Salen−P, also unveiling the better charge separation (Figures 4d and S19). All of the results above show that Co−Salen−P exhibits more efficient charge separation and transfer, thus explaining the higher photocatalytic performance for $H_2$ evolution.

## CONCLUSIONS

In summary, by covalent bonding of salen metal complexes and pyrene chromophores, we successfully synthesized two new porous polymers (Co−Salen−P and Fe−Salen−P) for photocatalytic $H_2$ evolution. Interestingly, they exhibit excellent catalytic performance in the absence of additional noble-metal photosensitizers and cocatalysts, especially the $H_2$ production rate of Co−Salen−P reaches as high as 542.5 $\mu$mol $g^{-1}$ $h^{-1}$, which is higher than a large amount of reported Pt-assisted photocatalytic systems. A series of photo/electrochemical characterization techniques demonstrate that the high photocatalytic activity of Co−Salen−P is due to the efficient charge separation and transfer. This work emphasizes the importance of a covalent strategy for preparing highly active photocatalysts for $H_2$ generation.

## EXPERIMENTAL SECTION

**Materials and Instrumentation.** All chemicals were commercially available and used without further purification. Powder XRD patterns were recorded on D8 ADVANCE X-ray diffractometers with Cu K$\alpha$ radiation ($\lambda$ = 1.54 Å). TGA was carried out on a Netzsch TG-209 Thermogravimetry Analyzer in an Ar atmosphere. $N_2$ sorption measurements were conducted at 77 K using a multistation specific surface micropore and vapor adsorption analyzer (BELSORP-Mas, Microtrac BEL, Japan). EDS mapping was acquired on an FEI-Quanta FEG 250 scanning electron microanalyzer. The contents of Co, Fe, and Pd were quantified by ICP-MS (iCAP RQ, Germany). UV−vis spectra were recorded on a UV−vis spectrophotometer (UV-3600, Shimadzu, Japan). XPS spectra were recorded on an X-ray spectrometer (ESCALAB 250 Xi spectrometer, Thermo Scientific) with Al K$\alpha$ as the excitation source. EDS mapping was acquired on an ultrahigh-resolution field emission scanning electron microanalyzer (FEI-Verios 460L). LC-MS was conducted using a Waters LC-MS system (UPLC I Class/Xevo G2-S QTOF). The $^1$H NMR spectrum was recorded on a nuclear magnetic resonance (NMR) (Bruker AVANCE AV III 400) spectrometer. PL spectra were measured with an F-4600 fluorescence spectrometer. TRPL spectra were acquired on an FLS1000 fluorescence spectrometer. Photocurrent, EIS, and Mott−Schottky plot measurements were performed on a CHI 760E electrochemical workstation. The catalytic product was analyzed by gas chromatography (GC-2014+ATF, 230C, Shimadzu, Japan) equipped with a thermal conductivity detector (TCD).

**Synthesis of $H_2L$.** $H_2L$ was synthesized according to the literature.[49] Typically, 402 mg of 5-bromo-2-hydroxybenzaldehyde and 108 mg of o-phenylenediamine were dissolved in 20 and 60 mL of ethanol, respectively. Then, the ethanol solution of *o*-phenylenediamine was added slowly to the ethanol solution of 5-bromo-2-hydroxybenzaldehyde and stirred at room temperature for 5 h. The orange powder was collected by filtration and washed with ethanol three times. Finally, $H_2L$ was obtained by vacuum-drying at 60 °C for 12 h

**Synthesis of M−Salen Complexes (M = Co and Fe).** 36.6 mg of $Co(ClO_4)_2{\cdot}6H_2O$ or $Fe(ClO_4)_3{\cdot}H_2O$ was dissolved in 5 mL of ethanol, which was added slowly to 15 mL of dichloromethane containing $H_2L$ (47.4 mg). The mixtures were stirred at room temperature for 6 h, which were further concentrated to 5 mL at 45 °C. Then, 30 mL of petroleum ether was added to the above solutions. Brown powder of the Co−Salen complex and green powder of the Fe−Salen complex were formed, which were collected by filtration and washed with petroleum ether three times. Finally, M−Salen complexes were obtained by vacuum-drying at 60 °C for 12 h

**Synthesis of Co−Salen−P and Fe−Salen−P.** 1,3,6,8-Tetraethynylpyrene was first synthesized according to the literature.[59] Then, Co−Salen−P and Fe−Salen−P were synthesized through the Sonogashira−Hagihara coupling reaction. Typically, 53 mg of Co−Salen or Fe−Salen, 30 mg of 1,3,6,8-tetraethynylpyrene, and 35 mg of tetrakis(triphenylphosphine)palladium were added to a mixed solvent of 10 mL of DMF and 12 mL of triethylamine. The above mixture was purged with Ar for 20 min, which was further stirred at 120 °C for 24 h. After cooling down to room temperature, the black powder of Co−Salen−P (yield: 49.8%) or brown powder of Fe−Salen−P (yield: 42.3%) was obtained by centrifugation and washed with DMF and methanol.

**Synthesis of Salen−P.** Salen−P was synthesized following the same procedure as Co−Salen−P except for the addition of $H_2L$ instead of Co−Salen. The orange powder of Salen−P (yield: 79.6%) was obtained (the content of Pd was 1.1%).

**Photocatalytic Measurement.** A photocatalytic $H_2$ evolution experiment was performed in a 16.5 mL glass reactor. A mixture of the photocatalyst (0.5 mg), ascorbic acid (88 mg), and $CH_3CN/H_2O$ (5 mL, v/v = 4:1) was added to the photoreactor. The reaction system was degassed with $N_2$ to remove $O_2$ and other gases, followed by 300 W Xe lamp irradiation ($\lambda$ > 320 nm). The generated gaseous products were analyzed with gas chromatography.

**Photoelectrochemical Measurements.** The photo/electrochemical measurements of Co−Salen−P and Fe−Salen−P were performed on a CHI 760E electrochemical workstation via a standard three-electrode system with a working electrode, a platinum wire as a counter electrode, and a saturated Ag/AgCl electrode as a reference electrode. A 300 W xenon lamp was used as the light source. 2.0 mg of Co−Salen−P or Fe−Salen−P was dispersed into a solution of 5.0 $\mu$L of 5 wt % Nafion, 0.75 mL of ethanol, and 0.25 mL of deionized water. Then, the solution was deposited onto the FTO surface and left in the air for drying to obtain the working electrode. The photocurrent and Mott−Schottky plot measurements were performed in 0.1 M $Na_2SO_4$, and EIS measurements were carried out in a 0.1 M


https://doi.org/10.1021/acs.inorgchem.4c01774
Inorg. Chem. 2024, 63, 13594−13601

$TBAPF_4$ MeCN/$H_2O$ (4:1) solution. The photocurrent was recorded at −0.4 V. EIS measurement was carried out at −0.6 V in the dark. Mott−Schottky plots were obtained at different frequencies (800 and 1200 Hz).

**DFT Calculations.** DFT calculations were performed by using the hybrid B3LYP-D3 functional with Grimme's D3 dispersion correction,[60] as implemented in the Gaussian16 program.[61] The self-consistent reaction field (SCRF) method was used during the calculations. All geometries were optimized with no constraint of freedom by using the SDD pseudopotential for the Co, 6-31G (d) basis set for C, N, O, and H elements.

## ■ ASSOCIATED CONTENT

### Supporting Information

The Supporting Information is available free of charge at https://pubs.acs.org/doi/10.1021/acs.inorgchem.4c01774.

Synthetic schematic diagram; $^1H$ NMR spectrum; LC-MS spectra; powder XRD patterns; EDS mapping; XPS spectra; pore size distributions; TGA curves; Tauc plots; Mott−Schottky plots; FTIR spectra; transient fluorescence lifetime; and reported Pt-assisted photocatalytic systems (PDF)

## ■ AUTHOR INFORMATION


### Corresponding Authors

**Ji-Hua Deng** − *Institute for New Energy Materials and Low Carbon Technologies, School of Materials Science and Engineering, School of Chemistry and Chemical Engineering, Tianjin University of Technology, Tianjin 300384, China*; Email: djhycu_2006@aliyun.com

**Yun-Nan Gong** − *Institute for New Energy Materials and Low Carbon Technologies, School of Materials Science and Engineering, School of Chemistry and Chemical Engineering, Tianjin University of Technology, Tianjin 300384, China*; orcid.org/0000-0002-9087-2261; Email: yngong@email.tjut.edu.cn

### Authors

**Shu-Ying Huang** − *Institute for New Energy Materials and Low Carbon Technologies, School of Materials Science and Engineering, School of Chemistry and Chemical Engineering, Tianjin University of Technology, Tianjin 300384, China*

**Xiao Lin** − *Institute for New Energy Materials and Low Carbon Technologies, School of Materials Science and Engineering, School of Chemistry and Chemical Engineering, Tianjin University of Technology, Tianjin 300384, China*

**Hao-Yu Yang** − *Institute for New Energy Materials and Low Carbon Technologies, School of Materials Science and Engineering, School of Chemistry and Chemical Engineering, Tianjin University of Technology, Tianjin 300384, China*

**Xue-Rong Dou** − *Institute for New Energy Materials and Low Carbon Technologies, School of Materials Science and Engineering, School of Chemistry and Chemical Engineering, Tianjin University of Technology, Tianjin 300384, China*

**Wen-Jie Shi** − *Institute for New Energy Materials and Low Carbon Technologies, School of Materials Science and Engineering, School of Chemistry and Chemical Engineering, Tianjin University of Technology, Tianjin 300384, China*

**Di-Chang Zhong** − *Institute for New Energy Materials and Low Carbon Technologies, School of Materials Science and Engineering, School of Chemistry and Chemical Engineering, Tianjin University of Technology, Tianjin 300384, China*

**Tong-Bu Lu** − *Institute for New Energy Materials and Low Carbon Technologies, School of Materials Science and Engineering, School of Chemistry and Chemical Engineering, Tianjin University of Technology, Tianjin 300384, China*; orcid.org/0000-0002-6087-4880

Complete contact information is available at: https://pubs.acs.org/10.1021/acs.inorgchem.4c01774

### Author Contributions

[†]S.-Y.H. and X.L. contributed equally to this work.


### Notes

The authors declare no competing financial interest.

## ■ ACKNOWLEDGMENTS

This work was supported by the National Key R&D Program of China (2022YFA1502902) and the National Natural Science Foundation of China (22371208, 22271218, 22071182, and 21931007).

## ■ REFERENCES


(1) Shakun, J. D.; Clark, P. U.; He, F.; Marcoot, S. A.; Mix, A. C.; Liu, Z.; Otto-Bliesner, B.; Schmittner, A.; Bard, E. Global warming preceded by increasing carbon dioxide concentrations during the last deglaciation. *Nature* **2012**, *484*, 49−54.

(2) Suremann, N. F.; McCarthy, B. D.; Gschwind, W.; Kumar, A.; Johnson, B. A.; Hammarström, L.; Ott, S. Molecular Catalysis of Energy Relevance in Metal-Organic Frameworks: From Higher Coordination Sphere to System Effects. *Chem. Rev.* **2023**, *123*, 6545−6611.

(3) Pitchaimani, J.; Ni, S.-F.; Dang, L. Metal dithiolene complexes in olefin addition and purification, small molecule adsorption, $H_2$ evolution and $CO_2$ reduction. *Coord. Chem. Rev.* **2020**, *420*, No. 213398.

(4) Ma, D.-D.; Han, S.-G.; Cao, C.; Wei, W.; Li, X.; Chen, B.; Wu, X.-T.; Zhu, Q.-L. Bifunctional single-molecular heterojunction enables completely selective $CO_2$-to-CO conversion integrated with oxidative 3D nano-polymerization. *Energy Environ. Sci.* **2021**, *14*, 1544−1552.

(5) Hu, M.-K.; Wang, N.; Ma, D.-D.; Zhu, Q.-L. Surveying the electrocatalytic $CO_2$-to-CO activity of heterogenized metallomacrocycles via accurate clipping at the molecular level. *Nano Res.* **2022**, *15*, 10070−10077.

(6) Wang, X.-Z.; Meng, S.-L.; Xiao, H.; Feng, K.; Wang, Y.; Jian, J.-X.; Li, X.-B.; Tung, C.-H.; Wu, L.-Z. Identifying a Real Catalyst of [NiFe]-Hydrogenase Mimic for Exceptional $H_2$ Photogeneration. *Angew. Chem., Int. Ed.* **2020**, *59*, 18400−18404.

(7) Su, L.; Luo, L.; Song, H.; Wu, Z.; Tu, W.; Wang, Z.-J.; Ye, J. Hemispherical shell-thin lamellar $WS_2$ porous structures composited with CdS photocatalysts for enhanced $H_2$ evolution. *Chem. Eng. J.* **2020**, *388*, No. 124346.

(8) Yuan, Y.; Pan, J.; Yin, W.; Yu, H.; Wang, F.; Hu, W.; Wang, L.; Yan, D. Effective strategies to promote Z(S)-scheme photocatalytic water splitting. *Chin. Chem. Lett.* **2024**, *35*, No. 108724.

(9) Pang, W.; Du, X.; Yang, Y.; Long, C.; Li, Y.; Hu, C.; Xu, R.; Tian, M.; Xie, J.; Wang, W.; Guo, J.; Li, B.; Zhang, P.; Fu, D.; Zhao, K. Oxygen Atom Coordinative Position Inducing Catalytic Sites Structure Reconstruction for Enhanced Photocatalytic $H_2$ Evolution. *Adv. Funct. Mater.* **2024**, *24*, No. 2400466.

(10) Li, J.; Feng, Y.; Fu, F.; Xin, X.; Yang, G.; Lv, H. Polyoxometalate-organic cage with $\{Ni_4SiW_9\}$ node for photocatalytic hydrogen evolution. *Chin. Chem. Lett.* **2024**, *35*, No. 108736.

(11) Dutta, S. A review on production, storage of hydrogen and it utilization as an energy resource. *J. Ind. Eng. Chem.* **2014**, *20*, 1148−1156.

(12) Li, X.; Lei, H.; Xie, L.; Wang, N.; Zhang, W.; Cao, R. Metalloporphyrins as Catalytic Models for Studying Hydrogen and Oxygen Evolution and Oxygen Reduction Reactions. *Acc. Chem. Res.* **2022**, *55*, 878−892.

(13) Shi, Y.; Zhang, B. Recent advances in transition metal phosphide nanomaterials: synthesis and applications in hydrogen evolution reaction. *Chem. Soc. Rev.* **2016**, *45*, 1529−1541.
(14) Nikoloudakis, E.; López-Duarte, I.; Charalambidis, G.; Ladomenou, K.; Ince, M.; Coutsolelos, A. G. Porphyrins and phthalocyanines as biomimetic tools for photocatalytic $H_2$ production and $CO_2$ reduction. *Chem. Soc. Rev.* **2022**, *51*, 6965−7045.
(15) Fu, Y.; Lu, K.; Hu, A.; Huang, J.; Guo, L.; Zhou, J.; Zhao, J.; Prezhdo, O. V.; Liu, M. $d_z^2$ Band Links Frontier Orbitals and Charge Carrier Dynamics of Single-Atom Cocatalyst-Aided Photocatalytic $H_2$ Production. *J. Am. Chem. Soc.* **2023**, *145*, 28166−28175.
(16) Wang, Y.; Zhang, Z.; Li, J.; Yuan, Y.; Yang, J.; Xu, W.; An, P.; Xi, S.; Guo, J.; Liu, B.; Li, J. Two-Dimensional-on-Three-Dimensional Metal-Organic Frameworks for Photocatalytic $H_2$ Production. *Angew. Chem., Int. Ed.* **2022**, *61*, No. e202211031, DOI: 10.1002/anie.202211031.
(17) Guan, X.; Qian, Y.; Zhang, X.; Jiang, H.-L. Enaminone-linked Covalent Organic Frameworks for Boosting Photocatalytic Hydrogen Production. *Angew. Chem., Int. Ed.* **2023**, *62*, No. e202306135.
(18) Lin, C.; Han, C.; Zhang, H.; Gong, L.; Gao, Y.; Wang, H.; Bian, Y.; Li, R.; Jiang, J. Porphyrin-Based Metal-Organic Frameworks for Efficient Photocatalytic $H_2$ Production under Visible-Light Irradiation. *Inorg. Chem.* **2021**, *60*, 3988−3995.
(19) Fujishima, A.; Honda, K. Electrochemical Photolysis of Water at a Semiconductor Electrode. *Nature* **1972**, *238*, 37−38.
(20) Kannan, K.; Chanda, D.; Gautam, J.; Behera, A.; Meshesha, M. M.; Jang, S. G.; Yang, B. L. Hydrothermally synthesized mixed metal oxide nanocomposites for electrochemical water splitting and photocatalytic hydrogen production. *Int. J. Hydrogen Energy* **2023**, *48*, 36412−36426.
(21) Ha, E.; Ruan, S.; Li, D.; Zhu, Y.; Chen, Y.; Qiu, J.; Chen, Z.; Xu, T.; Su, J.; Wang, L.; Hu, J. Surface disorder engineering in ZnCdS for cocatalyst free visible light driven hydrogen production. *Nano Res.* **2022**, *15*, 996−1002.
(22) Li, Y.; Zhuang, C.; Qiu, S.; Gao, J.; Zhou, Q.; Sun, Z.; Kang, Z.; Han, X. Cs-Cu-Cl perovskite quantum dots for photocatalytic $H_2$ evolution with super-high stability. *Appl. Catal., B* **2023**, *337*, No. 122881.
(23) Gong, Y.-N.; Guan, X.; Jiang, H.-L. Covalent organic frameworks for photocatalysis: Synthesis, structural features, fundamentals and performance. *Coord. Chem. Rev.* **2023**, *475*, No. 214889.
(24) Dhakshinamoorthy, A.; Li, Z.; Yang, S.; Garcia, H. Metal−organic framework heterojunctions for photocatalysis. *Chem. Soc. Rev.* **2024**, *53*, 3002−3035, DOI: 10.1039/d3cs00205e.
(25) Liu, N.; Jiang, J.; Chen, Z.; Wu, B.; Zhang, S.; Zhang, Y.-Q.; Cheng, P.; Shi, W. Promoted Photocatalytic Hydrogen Evolution by Tuning the Electronic State of Copper Sites in Metal-Organic Supramolecular Assemblies. *Angew. Chem., Int. Ed.* **2023**, *62*, No. e202312306, DOI: 10.1002/anie.202312306.
(26) Tang, Y.; Yuan, M.; Jiang, B.; Xiao, Y.; Fu, Y.; Chen, S.; Deng, Z.; Pan, Q.; Tian, C.; Fu, H. Inorganic acid-derived hydrogen-bonded organic frameworks to form nitrogen-rich carbon nitrides for photocatalytic hydrogen evolution. *J. Mater. Chem. A* **2017**, *5*, 21979−21985.
(27) Zhang, F.-M.; Sheng, J.-L.; Yang, Z.-D.; Sun, X.-J.; Tang, H.-L.; Lu, M.; Dong, H.; Shen, F.-C.; Liu, J.; Lan, Y.-Q. Rational Design of MOF/COF Hybrid Materials for Photocatalytic $H_2$ Evolution in the Presence of Sacrificial Electron Donors. *Angew. Chem., Int. Ed.* **2018**, *57*, 12106−12110.
(28) Li, Z.; Deng, T.; Ma, S.; Zhang, Z.; Wu, G.; Wang, J.; Li, Q.; Xia, H.; Yang, S.-W.; Liu, X. Three-Component Donor-$\pi$-Acceptor Covalent-Organic Frameworks for Boosting Photocatalytic Hydrogen Evolution. *J. Am. Chem. Soc.* **2023**, *145*, 8364−8374.
(29) Wang, S.; Ai, Z.; Niu, X.; Yang, W.; Kang, R.; Lin, Z.; Waseem, A.; Jiao, L.; Jiang, H.-L. Linker Engineering of Sandwich-Structured Metal-Organic Framework Composites for Optimized Photocatalytic $H_2$ Production. *Adv. Mater.* **2023**, *35*, No. 2302512.
(30) Ghosh, S.; Nakada, A.; Springer, M. A.; Kawaguchi, T.; Suzuki, K.; Kaji, H.; Baburin, I.; Kuc, A.; Heine, T.; Suzuki, H.; Abe, R.; Seki, S. Identification of Prime Factors to Maximize the Photocatalytic Hydrogen Evolution of Covalent Organic Frameworks. *J. Am. Chem. Soc.* **2020**, *142*, 9752−9762.
(31) Tang, S.; Xia, Y.; Fan, J.; Cheng, B.; Yu, J.; Ho, W. Enhanced photocatalytic $H_2$ production performance of CdS hollow spheres using C and Pt as bi-cocatalysts. *Chin. J. Catal.* **2021**, *42*, 743−752.
(32) Lv, Z.; Liu, P.; Zhao, Y.; Peng, C.; Meng, X.-Y.; Pan, Y.-X. Visible-light-driven photocatalytic $H_2$ production from $H_2O$ boosted by anchoring Pt and CdS nanoparticles on a NaY zeolite. *Chem. Eng. Sci.* **2022**, *255*, No. 117658.
(33) Zuo, Q.; Liu, T.; Chen, C.; Ji, Y.; Gong, X.; Mai, Y.; Zhou, Y. Ultrathin Metal−Organic Framework Nanosheets with Ultrahigh Loading of Single Pt Atoms for Efficient Visible-Light-Driven Photocatalytic $H_2$ Evolution. *Angew. Chem., Int. Ed.* **2019**, *58*, 10198−10203.
(34) Shi, X.; Dai, C.; Wang, X.; Hu, J.; Zhang, J.; Zheng, L.; Mao, L.; Zheng, H.; Zhu, M. Protruding Pt single-sites on hexagonal $ZnIn_2S_4$ to accelerate photocatalytic hydrogen evolution. *Nat. Commun.* **2022**, *13*, No. 1287.
(35) Wu, S.-M.; Hwang, I.; Osuagwu, B.; Will, J.; Wu, Z.; Sarma, B. B.; Pu, F.-F.; Wang, L.-Y.; Badura, Z.; Zoppellaro, G.; Spiecker, E.; Schmuki, P. Fluorine Aided Stabilization of Pt Single Atoms on $TiO_2$ Nanosheets and Strongly Enhanced Photocatalytic $H_2$ Evolution. *ACS Catal.* **2023**, *13*, 33−41.
(36) Wang, Z.; Wang, L.; Cheng, B.; Yu, H.; Yu, J. Photocatalytic $H_2$ Evolution Coupled with Furfuralcohol Oxidation over Pt-Modified ZnCdS Solid Solution. *Small Methods* **2021**, *5*, No. 2100979.
(37) Zhang, L.; Fu, X.; Meng, S.; Jiang, X.; Wang, J.; Chen, S. Ultra-low content of Pt modified CdS nanorods: one-pot synthesis and high photocatalytic activity for $H_2$ production under visible light. *J. Mater. Chem. A* **2015**, *3*, 23732−23742.
(38) Wang, G.; Zhang, C.; Zhao, W.; Wang, B.; Liu, Y.; Zhang, T.; Cui, W.; Zhang, R.; Zhao, Z. Bonding Interaction of Adjacent Pt and Ag Single-Atom Pairs on Carbon Nitride Efficiently Promotes Photocatalytic $H_2$ Production. *CCS Chem.* **2024**, *6*, 1523−1534.
(39) Gueret, R.; Poulard, L.; Oshinowo, M.; Chauvin, J.; Dahmane, M.; Dupeyre, G.; Laine, P. P.; Fortage, J. P.; Collomb, M.-N. Challenging the $[Ru(bpy)_3]^{2+}$ Photosensitizer with a Triazatriangulenium Robust Organic Dye for Visible-Light-Driven Hydrogen Production in Water. *ACS Catal.* **2018**, *8*, 3792−3802.
(40) Rao, H.; Yu, W.-Q.; Zheng, H.-Q.; Bonin, J.; Fan, Y.-T.; Hou, H.-W. Highly efficient photocatalytic hydrogen evolution from nickel quinolinethiolate complexes under visible light irradiation. *J. Power Sources* **2016**, *324*, 253−260.
(41) Kong, X.; Gao, Z.; Gong, Y.; Huang, H.; Wang, H.; Liu, P.; Yin, H.; Cui, Z.; Li, Z.; Liang, Y.; Zhu, S.; Huang, Y.; Yang, X. Enhancement of photocatalytic $H_2$ production by metal complex electrostatic adsorption on $TiO_2$ (B) nanosheets. *J. Mater. Chem. A* **2019**, *7*, 3797−3804.
(42) Zhang, W.; Gu, Q.; Fu, X.; Wang, Y.; Jian, Y.; Sun, H.; Gao, Z. Regulating CO and $H_2$ Ratios in Syngas Produced from Photocatalytic $CO_2/H_2O$ Reduction by Cu and Co Dual Active Centers on Carbon Nitride Hollow Nanospheres. *Inorg. Chem.* **2023**, *62*, 13615−13625.
(43) Xie, A.; Zhu, J.; Luo, G.-G. Efficient electrocatalytic and photocatalytic hydrogen evolution using a linear trimeric thiolato complex of nickel. *Int. J. Hydrogen Energy* **2018**, *43*, 2772−2780.
(44) Li, C.-B.; Chu, Y.; He, J.; Xie, J.; Liu, J.; Wang, N.; Tang, J. Photocatalytic Hydrogen Production Based on a Serial Metal-Salen Complexes and the Reaction Mechanism. *ChemCatChem* **2019**, *11*, 6324−6331.
(45) Yang, G.-L.; Xie, Y.; Jiao, Z.-H.; Zhao, J.; Hou, S.-L.; Shi, Y.; Han, J.; Zhao, B. A strong-alkali resistant zinc−organic framework with 1,3,6,8-tetra(pyridin-4-yl)pyrene for efficient photocatalytic hydrogen evolution. *J. Mater. Chem. A* **2023**, *11*, 16255−16262.
(46) Wang, L.; Chakraborty, J.; Deng, M.; Sun, J.; Voort, P. V. D. Donor-Acceptor Pyrene-Based Covalent Organic Framework for Blue Light Photocatalytic Oxidative Coupling of Amines. *ChemCatChem.* **2024**, No. e202400200, DOI: 10.1002/cctc.202400200.

(47) Luo, Z.; Chen, X.; Hu, Y.; Chen, X.; Lin, W.; Wu, X.; Wang, X. Side-Chain Molecular Engineering of Triazole-Based Donor-Acceptor Polymeric Photocatalysts with Strong Electron Push-Pull Interactions. *Angew. Chem., Int. Ed.* **2023**, *62*, No. e202304875.
(48) Wang, X.; Ma, K.; Goh, T.; Mian, M. R.; Xie, H.; Mao, H.; Duan, J.; Kirlikovali, K. O.; Stone, A. E. B. S.; Ray, D.; Wasielewski, M. R.; Gagliardi, L.; Farha, O. K. Photocatalytic Biocidal Coatings Featuring $Zr_6Ti_4$-Based Metal-Organic Frameworks. *J. Am. Chem. Soc.* **2022**, *144*, 12192−12201.
(49) Zhou, W.; Wang, X.; Zhao, W.; Lu, N.; Cong, D.; Li, Z.; Han, P.; Ren, G.; Sun, L.; Liu, C.; Deng, W.-Q. Photocatalytic $CO_2$ reductiontosyngasusing metallosalen covalent organic frameworks. *Nat. Commun.* **2023**, *14*, No. 6971.
(50) Zhou, W.; Shen, H.; Zeng, Y.; Yi, Y.; Zuo, Z.; Li, Y.; Li, Y. Controllable Synthesis of Graphdiyne Nanoribbons. *Angew. Chem., Int. Ed.* **2020**, *59*, 4908−4913.
(51) Li, J.; Gao, X.; Liu, B.; Feng, Q.; Li, X.-B.; Huang, M.-Y.; Liu, Z.; Zhang, J.; Tung, C.-H.; Wu, L.-Z. Graphdiyne: A Metal-Free Material as Hole Transfer Layer To Fabricate Quantum Dot-Sensitized Photocathodes for Hydrogen Production. *J. Am. Chem. Soc.* **2016**, *138*, 3954−3957.
(52) Gong, Y.-N.; Zhong, W.; Li, Y.; Qiu, Y.; Zheng, L.; Jiang, J.; Jiang, H.-L. Regulating Photocatalysis by Spin-State Manipulation of Cobalt in Covalent Organic Frameworks. *J. Am. Chem. Soc.* **2020**, *142*, 16723−16731.
(53) Chubar, N.; Gerda, V.; Szlachta, M.; Yablokova, G. Effect of Fe oxidation state (+2 versus + 3) in precursor on the structure of Fe oxides/carbonates-based composites examined by XPS, FTIR and EXAFS. *Solid State Sci.* **2021**, *121*, No. 106752.
(54) Li, Q.; Chang, J.-N.; Wang, Z.-M.; Lu, M.; Guo, C.; Zhang, M.; Yu, T.-Y.; Chen, Y.; Li, S.-L.; Lan, Y.-Q. Modulated Connection Modes of Redox Units in Molecular Junction Covalent Organic Framework for Artificial Photosynthetic Overall Reaction. *J. Am. Chem. Soc.* **2023**, *145*, 23167−23175.
(55) Sun, K.; Qian, Y.; Jiang, H.-L. Metal-Organic Frameworks for Photocatalytic Water Splitting and $CO_2$ Reduction. *Angew. Chem., Int. Ed.* **2023**, *62*, No. e202217565, DOI: 10.1002/anie.202217565.
(56) Liu, H.; Xu, C.; Li, D.; Jiang, H.-L. Photocatalytic Hydrogen Production Coupled with Selective Benzylamine Oxidation over MOF Composites. *Angew. Chem., Int. Ed.* **2018**, *57*, 5379−5383.
(57) Gong, Y.-N.; Shao, B.-Z.; Mei, J.-H.; Yang, W.; Zhong, D.-C.; Lu, T.-B. Facile synthesis of $C_3N_4$-supported metal catalysts for efficient $CO_2$ photoreduction. *Nano Res.* **2022**, *15*, 551−556.
(58) Yang, Y.; Zhang, H.-Y.; Wang, Y.; Shao, L.-H.; Fang, L.; Dong, H.; Lu, M.; Dong, L.-Z.; Lan, Y.-Q.; Zhang, F.-M. Integrating Enrichment, Reduction and Oxidation Sites in One System for Artificial Photosynthetic Diluted $CO_2$ Reduction. *Adv. Mater.* **2023**, *35*, No. 2304170.
(59) Li, G.; Li, Y.; Liu, H.; Guo, Y.; Li, Y.; Zhu, D. Architecture of graphdiyne nanoscale films. *Chem. Commun.* **2010**, *46*, 3256−3258.
(60) Grimme, S.; Ehrlich, S.; Goerigk, L. Effect of the damping function in dispersion corrected density functional theory. *J. Comput. Chem.* **2011**, *32*, 1456−1465.
(61) Frisch, M.-J.; Trucks, G.-W.; Schlegel, H.-B.; Scuseria, G.-E.; Robb, M.-A.; Cheeseman, J.-R.; Scalmani, G.; Barone, V.; Petersson, G.-A.; Nakatsuji, H. *Gaussian*; Gaussian, Inc.: Wallingford, CT, 2016.


https://doi.org/10.1021/acs.inorgchem.4c01774
*Inorg. Chem.* 2024, 63, 13594−13601